nature neuroscience

A critical period for auditory thalamocortical connectivity

Tania Rinaldi Barkat[1], Daniel B Polley[2] & Takao K Hensch[1]

Neural circuits are shaped by experience during periods of heightened brain plasticity in early postnatal life. Exposure to acoustic features produces age-dependent changes through largely unresolved cellular mechanisms and sites of origin. We isolated the refinement of auditory thalamocortical connectivity by *in vivo* recordings and day-by-day voltage-sensitive dye imaging in an acute brain slice preparation. Passive tone-rearing modified response strength and topography in mouse primary auditory cortex (A1) during a brief, 3-d window, but did not alter tonotopic maps in the thalamus. Gene-targeted deletion of a forebrain-specific cell-adhesion molecule (*Icam5*) accelerated plasticity in this critical period. Consistent with its normal role of slowing spinogenesis, loss of *Icam5* induced precocious stubby spine maturation on pyramidal cell dendrites in neocortical layer 4 (L4), identifying a primary locus of change for the tonotopic plasticity. The evolving postnatal connectivity between thalamus and cortex in the days following hearing onset may therefore determine a critical period for auditory processing.

Neural circuits are shaped by experience during periods of heightened brain plasticity in early life[1,2]. Children raised in an English-speaking environment easily distinguish between the phonemes /la/ and /ra/, whereas those growing up in Japan find it increasingly difficult[3]. Passive exposure of young rodents to a variety of sound features reveals a cascading series of developmental windows that open and close shortly after hearing onset to define the persistent and specific influences of early experience on the functional organization of auditory cortex[4–6]. The underlying sites of plasticity along the auditory pathway, as well as potential mechanisms engaged during such critical periods, remain unknown.

Motivated by the well known binocular interactions shaped by experience in developing visual cortex[7–9], we used *in vivo* neurophysiological recordings to determine whether mouse A1 also exhibits a critical period for tonotopic map plasticity induced through passive tone exposure, and whether such plasticity is present in the auditory thalamus (ventral medial geniculate body, MGBv). We then isolated the connection between MGBv and primary auditory cortex (A1) (ref. 10) in an acute brain slice preparation[11] and used voltage-sensitive dye imaging (VSDI) techniques *in vitro*. We mapped A1 responses to electrical stimulation of discrete sites in MGBv across early postnatal days (P8–20), following tone-rearing or gene manipulation. Our results reveal a critical period for acoustically driven topographic plasticity at thalamocortical connections in mouse A1.

RESULTS

Tone exposure modifies tonotopic maps in A1, but not MGBv

The auditory system is tonotopically organized[10] such that tones of similar frequency activate neighboring neurons at each station along the pathway. Given that rats show experience-dependent tonotopic map reorganization following passive tone exposure during the second postnatal week[2,12], we first used high-density *in vivo* mapping to delineate A1 tonotopy in young adult mice[13] that were reared either in typical acoustic environments (**Fig. 1a**) or in the presence of pulsed 7-kHz tone pips from P11 to P15 (**Fig. 1b**) or P16 to P20 (**Fig. 1c**). Comparison of representative tonal receptive fields drawn from caudal, intermediate and rostral map locations (**Fig. 1d**) revealed that tone-rearing from P11 to P15, but not P16 to P20, was sufficient to shift A1 best frequencies toward the 7-kHz exposure frequency (P11–15 versus exposure, $n = 5$ mice and 93 sites for each group, $P = 0.003$; P16–20, 4 mice and 64 sites versus no exposure, $P = 1.0$, Kolmogorov-Smirnov test; **Fig. 1e**). On closer inspection, the expansion of best frequency representations near the exposure frequency was attributable to topographically specific reallocation of best frequencies in caudal and intermediate regions of the tonotopic map proximal to where 7 kHz is normally represented, rather than a shift in more rostral map areas that retain normal tuning to higher frequencies ($P = 0.009$, 0.04 and 0.14 for P11–15 versus no exposure at caudal, mid and rostral locations, respectively, *t* test; **Fig. 1f**,**g**).

To determine whether remapping in A1 could be explained by a shifted frequency representation in the principal subcortical input source, we also examined best frequency distributions in the MGBv. We inserted a multichannel silicon probe at an angle that matched the plane of section used in subsequent thalamocortical slice experiments[13] (**Fig. 2a**). This approach allowed us to sample the low-to-high, lateral-to-medial best frequency gradient in MGBv *in vivo* (**Fig. 2b**) with a comparable multi-unit signal-to-noise ratio as in our A1 recordings (**Fig. 2c**) while excluding recordings from auditory areas medial to MGBv (**Fig. 2d** and Online Methods). Although 7-kHz rearing from P11–15 induced a significant shift in A1 maps (**Fig. 1**), we found no evidence for shifts in overall best frequency distributions in MGBv (P11–15, $n = 5$ mice and 151 sites versus no exposure, $n = 4$ mice and 101 sites; $P = 0.99$, Kolmogorov-Smirnov test; **Fig. 2e**) or differences in mean best frequency at lateral (50 µm into MGBv), more medial (200 µm into MGBv) or across all recording sites ($P = 0.44$, 0.18 and 0.91 at lateral, medial and overall locations, respectively, *t* test; **Fig. 2f**). In contrast, other auditory receptive field changes, such as best frequency–specific reductions in tuning

[1]Center for Brain Science, Department of Molecular and Cellular Biology, Harvard University, Cambridge, Massachusetts, USA. [2]Eaton-Peabody Laboratory, Massachusetts Eye and Ear Infirmary, Department of Otology and Laryngology, Harvard Medical School, Boston, Massachusetts, USA. Correspondence should be addressed to T.K.H. (hensch@mcb.harvard.edu).

Received 1 April; accepted 6 June; published online 31 July 2011; doi:10.1038/nn.2882

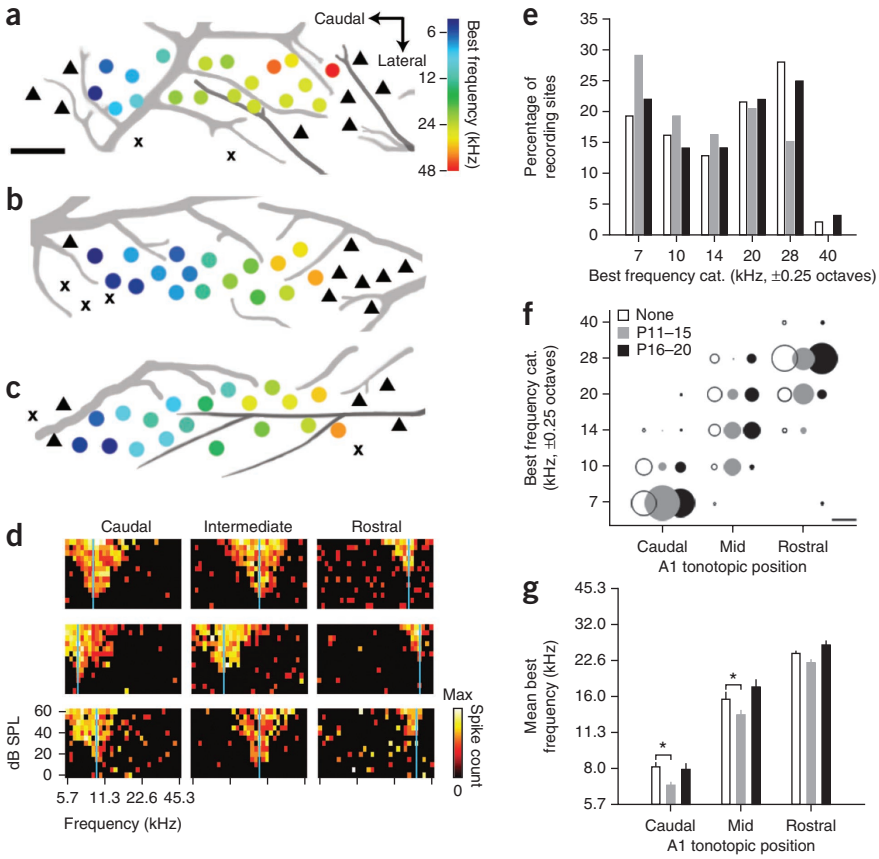

Figure 1 Developmental cortical map reorganization in mouse A1. (**a**–**c**) Representative A1 best frequency maps from the left hemisphere of young adult mice (P32–39) reared in a normal sound environment (**a**) or after 7-kHz tone exposure between P11–15 (**b**) or P16–20 (**c**). Circle denotes multi-unit recording site and hue represents best frequency (color scale). Triangles indicate non-A1 recording sites and x's indicate non-responsive sites. Scale bar represents 0.25 mm. Dark and light gray lines represent branches of the middle cerebral artery and inferior branches of the rhinal vein, respectively. (**d**) Sample frequency response areas of normalized firing rates as a function of tone frequency and level. Recordings obtained from caudal, intermediate and rostral zones of A1 from mice reared in a normal sound environment (top) or with 7-kHz tones between P11–15 (middle) or P16–20 (bottom). Vertical blue lines indicate best frequency. (**e**) Percentage of recording sites of all best frequency measurements in normally reared mouse A1 (open bars; $n = 18, 15, 12, 20, 26$ and 2 sites for each of the six categories (cat.)) or those reared with 7-kHz tones between P11–15 (gray bars; $n = 27, 18, 15, 19, 14$ and 0 sites) or P16–20 (black bars, $n = 14, 9, 9, 14, 16$ and 2 sites). Best frequencies are grouped into 0.5-octave bins centered on the x axis frequency. (**f**) Best frequency distributions segregated by rearing condition and topographic location. The percentages of best frequency sites are represented by circle diameter. Scale bar denotes a diameter equaling 50% of the distribution. (**g**) Best frequency values (mean ± s.e.m.) for each rearing group and topographic position. $^*P < 0.05$ (t test).

bandwidth, were found in both MGBv recordings (P11–15) and throughout A1 (P11–20) (**Supplementary Fig. 1**).

A developmental time window for A1 response maturation

In the rodent MGBv, the gradient of preferred sound from low (lateral) to high (medial) frequency allows us to mimic tones of varying frequency across the latero-medial axis *in vitro*[13–15]. We stimulated the MGBv at six different loci along this dimension in brain slices, preserving the thalamocortical connection to A1 (**Fig. 3a**)[11], and used VSDI to measure cortical response (**Supplementary Fig. 2**). Discrete current pulses to MGBv yielded topographically distinct, maximal responses across upper L4 of A1 that we used to derive a map of peak amplitudes as function of stimulus site (L4 loci; **Fig. 3a**)[13].

In young animals (P8–12), responses to lateral MGBv loci were significantly weaker than responses to medial stimuli (peak $\Delta F/F$ at locus 1, 0.30 ± 0.06; locus 6, 0.82 ± 0.05; $n = 13$ each, $P < 0.00001$, t test; **Fig. 3b**). This inhomogeneous distribution of peak amplitudes gradually disappeared with brain maturation. After P15, peak cortical

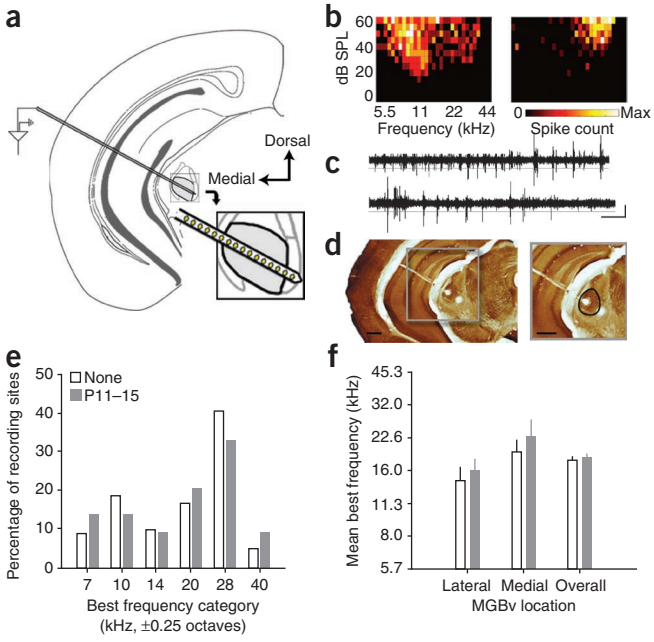

Figure 2 Thalamic tonotopy remains stable despite reorganization of A1 maps. (**a**) *In vivo* recordings from MGBv (gray shading) with a multichannel silicon probe inserted at an angle matching the plane of thalamocortical slices. Inset, schematic depicting position of recording sites relative to cytoarchitectonic boundaries of MGBv. (**b**) Representative frequency response areas recorded from a lateral (left) and medial (right) recording site in MGBv. All conventions match those in **Figure 1d**. (**c**) Examples of raw multi-unit traces recorded with a tungsten microelectrode used for A1 mapping (upper) or silicon probe used for MGBv mapping (lower). Spikes were registered when signal amplitude exceeded a threshold line set at 4 s.d. from the mean of a 5-s running average (indicated by gray line). Scale bars represent 1 s and 0.1 mV. (**d**) Images of coronal section through MGBv reacted for cytochrome oxidase. High-power image depicts the location of two lesions made inside and outside of the MGBv boundary (black outline). Scale bars represent 0.5 mm. (**e**) Percentage of recording sites of all best frequency measurements from normally reared mouse MGBv (open bars; $n = 9, 19, 10, 17, 41$ and 5 sites for each of the six categories) and those reared with 7-kHz tones between P11–15 (gray bars; $n = 21, 21, 14, 31, 50$ and 14 sites). (**f**) Best frequency values (mean ± s.e.m.) measured at lateral (0.05 mm past the lateral MGBv boundary) or medial loci (0.2 mm past the lateral MGBv boundary), as well as averaged overall.

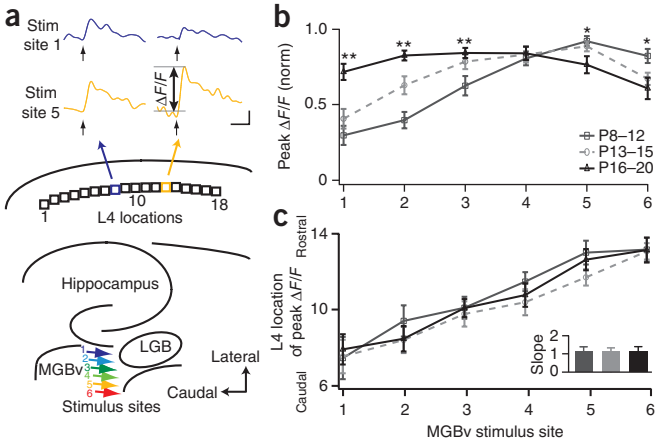

Figure 3 Topography and developmental window for A1 response strengthening at P12–15. (**a**) Schematic of the six MGBv stimulus (stim) sites (colored arrows) and 18 L4 locations analyzed in A1. Sample traces of $\Delta F/F$ at two different L4 loci (8 and 13) as a function of time following a 1-ms stimulus pulse to MGBv site 1 (blue) or 5 (yellow). P12 control mouse. Scale bars represent 100 ms and 0.1% $\Delta F/F$. (**b**) Normalized (norm) peak $\Delta F/F$ as a function of stimulus site for three age groups (mean ± s.e.m.; P8–12, $n = 13$; P13–15, $n = 16$; P16–20, $n = 16$). $^{*}P < 0.05$, $^{**}P < 0.01$ (t test) between dark gray and black. (**c**) Peak $\Delta F/F$ location in L4 as a function of MGBv stimulus site. Inset, topographic slope (mean ± s.e.m.) for the three age groups.

responses were similar across stimulus sites (**Fig. 3b**). Notably, the adjustment of thalamocortical response strength occurred in 3 d, between P12 and P15, coinciding with the emergence of adult-like A1 neural response thresholds for airborne sound transmission[6,16]. We validated these thalamocortical modifications over development at synaptic resolution by direct patch-clamp recording from upper L4 pyramidal neurons in mice before P12 and comparing the results with those from mice after P15 (**Supplementary Fig. 3**).

Notably, the mapping of peak response in L4 as a function of MGBv stimulus site did not change during the developmental period that we studied (P8–20). As indicated by the linear relation of peak $\Delta F/F$ position in L4 to MGBv input (topographic slope; **Fig. 3c**), an orderly spatial layout of this pathway was already present before hearing onset[16], even as connection strengths were still maturing across the map (**Fig. 3b**).

A critical period for thalamocortical connectivity

Normal acoustic experience therefore did not modify the intrinsic organization of thalamocortical input present at hearing onset. In contrast, if the mice were exposed early to an abnormal acoustic environment, the topography was markedly altered. Maximal A1 responses along the rostro-caudal L4 axis in P16–20 mice were concentrated near a single, middle MGBv input after continuous exposure to 7-kHz tone pips from P8 (**Fig. 4a**,**b**). Although the strength of cortical responses retained homogeneity across stimulus sites, a clear flattening of topographic slope was evident in L4 (**Fig. 4c**). This direct functional rearrangement of thalamocortical response was confirmed by comparing the distributions of input strength for two independent stimulus sites (1 and 6) (control, $P = 0.003$; exposed, $P = 0.181$; ANOVA), as well as the gradient of peak locations ($P = 0.029$, ANOVA), in control and exposed mice.

We exposed mice to 7-kHz tones for shorter, 3-d intervals (P8–11, P12–15 and P16–19; **Fig. 4d**) and found significant topographic reorganization only when mice were exposed from P12–15 (topographic slope at P20, no exposure = 1.42 ± 0.37, $n = 9$; versus P12–15, exposure = 0.07 ± 0.13, $n = 8$; $P = 0.026$, Mann-Whitney U test; **Fig. 4e**). This identified a critical period for mouse auditory thalamocortical topography that coincides with the normal time window during which this connection is maturing (**Fig. 3b**) and for tonotopic map changes *in vivo* (**Fig. 1**). Topographic remapping was not restricted to 7 kHz, as passive tone exposure to 20 kHz (from P12–15) produced a similar topographic reorganization at a correspondingly more rostral A1 locus (**Supplementary Fig. 4**).

Laminar shift of connectivity during the critical period

We further examined the emergence of A1 responses along a cortical column during postnatal development. As expected, the maximum response amplitude to MGBv stimulation was located in upper L4 at 325 ± 75 µm from the pial surface for all of the ages that we studied (**Fig. 5a**). Although each thalamocortical preparation was unique, the variability in geometry and size of various anatomical hallmarks relative to a reference point (the rostral tip of the hippocampus; **Supplementary Fig. 5**) was small across the developmental period studied (**Supplementary Fig. 5**). Notably, changes in total cortical thickness across these ages were negligible (<10 µm per bin) with respect to the individual bin sizes. However, the location of shortest response latency shifted

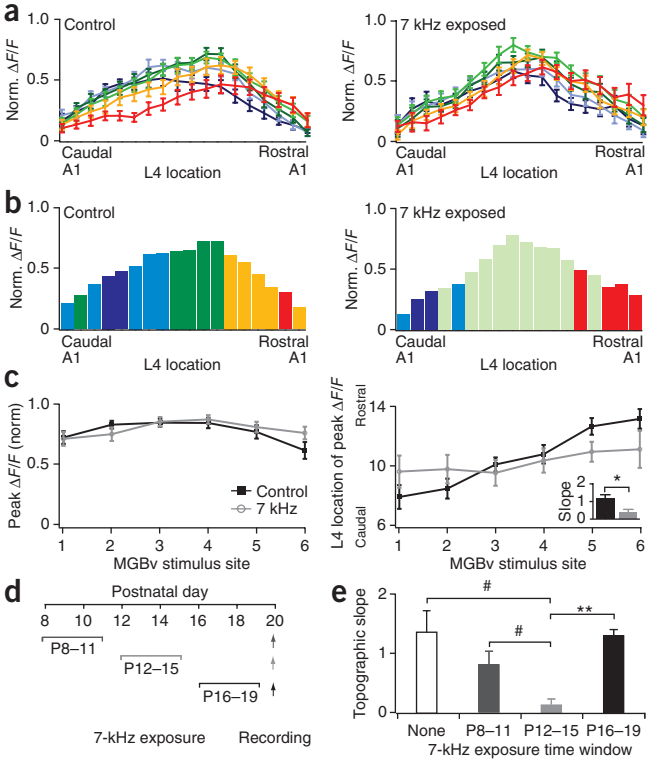

Figure 4 Critical period for experience-dependent topographic refinement at P12–15. (**a**,**b**) Normalized (norm.) maximal $\Delta F/F$ across L4 loci in response to different MGBv stimulus sites for P16–20 mice raised in a normal acoustic environment (left, $n = 16$) or exposed to a 7-kHz tone from P8 (right, $n = 13$). Color code indicates MGBv stimulus site as in **Figure 3a**. (**c**) Normalized peak $\Delta F/F$, defined as the maximum $\Delta F/F$ amplitude across all L4 loci, and location of L4 peak $\Delta F/F$ in response to different MGBv stimulus site for P16–20 control and 7-kHz exposed mice. Inset, topographic slopes. Data are mean ± s.e.m., $^{*}P < 0.05$ (t test). (**d**) Schedule of tone exposure windows and recording (arrows). (**e**) Topographic slopes (median ± s.e.m.) for control mice (none, $n = 9$) and those exposed to 7 kHz during three time windows (P8–11, $n = 8$; P12–15, $n = 8$; P16–19, $n = 5$). $^{\#}P < 0.05$, $^{**}P < 0.01$ (Mann-Whitney U test).

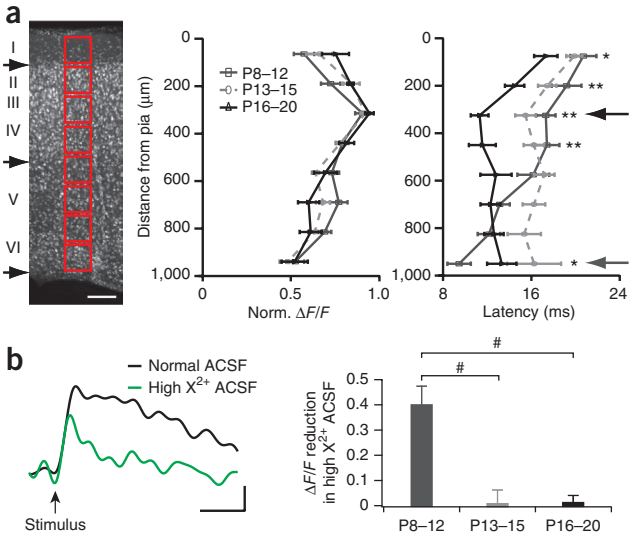

Figure 5 Columnar shift of thalamocortical connectivity up to L4 through the critical period. (**a**) Nissl stain of a P20 thalamocortical slice for columnar analysis (red boxes). Black arrows denote approximate borders between layers I/II, layers IV/V and layer VI/white matter. Scale bar represents 125 μm. Normalized (norm.) $\Delta F/F$ and latency with distance from pia for three age groups (mean ± s.e.m.; P8–12, $n = 13$; P13–15, $n = 15$; P16–20, $n = 11$). $^{*}P < 0.05$, $^{**}P < 0.01$ (t test) between dark gray and black. (**b**) Sample upper L4 cortical response at P10 in normal (black) and high X^{2+} (green) ACSF. Scale bars represent 100 ms and 0.2% $\Delta F/F$. Response reduction (median ± s.e.m.) in high X^{2+} for three age groups (P8–12, $n = 6$; P13–15, $n = 8$; P16–20, $n = 4$). $^{\#}P < 0.05$ (Mann-Whitney U test).

significantly upward along the column over the course of the critical period for plasticity (minimum latency site, P8–11 = 900 ± 75 μm, P16–20 = 325 ± 75 μm, $P < 0.0001$, t test; **Fig. 5a**). This was true across the entire rostro-caudal extent of A1 (**Supplementary Fig. 6**).

Moreover, when polysynaptic activity was weakened in a modified (high divalent cation, X^{2+}) artificial cerebrospinal fluid (ACSF)[11], the strong signal observed in upper L4 was significantly reduced at P8–12, but not in older animals $(\Delta F/F_{normal} - \Delta F/F_{high\ x2+})/(\Delta F/F_{normal})$: P8–12, 0.40 ± 0.13, $n = 6$; versus P13–15, 0.01 ± 0.06, $n = 8$, $P = 0.020$; versus P16–20, 0.01 ± 0.05, $n = 4$, $P = 0.038$, Mann-Whitney U test; **Fig. 5b**). Tone exposure did not affect this upward translocation of direct thalamocortical input to L4, as there was little reduction of peak signal in high divalent cation ACSF for mice that were passively exposed to 7 kHz (P16–20 = 0.11 ± 0.19, $n = 4$). These results indicate that thalamic inputs initially target their synapses to deeper regions, most probably the subplate (a transient zone in the developing neocortex)[17–19], before invading L4 during the critical period.

Forebrain-selective gene deletion accelerates plasticity

To establish a thalamocortical mechanism for this critical period plasticity, we analyzed a mouse model carrying a forebrain-specific gene deletion of *Icam5*, which is an intercellular adhesion molecule that is expressed exclusively in the telencephalon[20] and is sorted into dendrites of pyramidal cells to slow spine maturation[21] (**Fig. 6a**). Notably, *Icam5* was not expressed in the MGBv or other subcortical structures in wild-type animals, and was absent throughout the brain of *Icam5*$^{-/-}$ mice (**Fig. 6b**).

Consistent with *Icam5* being a negative regulator of spine maturation, peak A1 response strength in upper L4 of *Icam5*$^{-/-}$ mice matured rapidly to a homogeneous distribution in just 1 d, from P12 to P13 (**Fig. 6c**), unlike the typical 3 d that is needed in wild-type mice (**Fig. 3b**). By P13, *Icam5*$^{-/-}$ mice already exhibited a fully mature amplitude distribution that was comparable to that of P16 wild-type mice (**Supplementary Fig. 7a**). Moreover, the upward shift of columnar response latencies occurred faster in *Icam5*$^{-/-}$ mice and was also mature by P13 (**Supplementary Fig. 7b**). These animals exhibit stronger long-term potentiation and hippocampal learning behavior[20], suggesting that a similar mechanism may be at work for thalamocortical synapses in L4.

As the period of normal circuit maturation corresponds to the critical period for topographic changes in wild-type mice (**Figs. 3b** and **4e**), we tested whether plasticity would also be accelerated in *Icam5*$^{-/-}$ mice. The topography of *Icam5*$^{-/-}$ mice was identical to that of wild-type mice when they were raised in normal acoustic environments (**Fig. 6d**). However, exposing the mice to 7-kHz tones for just 1 d (P12–13) significantly altered topography at P16–20 in *Icam5*$^{-/-}$ mice, but not in wild-type mice (topographic slope: wild type, 0.86 ± 0.20, $n = 9$; *Icam5*$^{-/-}$, 0.23 ± 0.10, $n = 7$; $P = 0.014$, Mann-Whitney U test; **Fig. 6d**). Even 2 d of exposure were insufficient to yield topographic changes in wild-type mice (P12–14 or P13–15; **Supplementary Fig. 7c**).

Exposing *Icam5*$^{-/-}$ mice between P13–14 also altered topography, but to a lesser extent than at P12–13 (topographic slope: *Icam5*$^{-/-}$ not exposed, 0.97 ± 0.03, $n = 9$; *Icam5*$^{-/-}$ exposed between P13–14, 0.25 ± 0.22, $n = 9$; $P = 0.048$, Mann-Whitney U test; **Fig. 6d**). Even later exposure between P14–15 (**Fig. 6d**) or before the typical critical period (P8–11, **Supplementary Fig. 7c**) did not cause any significant change in the topographic organization of *Icam5*$^{-/-}$ mice ($P = 0.70$ or 0.22 between non-exposed and P14–15 or P8–11 exposed, respectively; Mann-Whitney U test). Thus, the critical period itself is not shifted earlier in time, but is instead shortened in duration in the absence of forebrain-specific *Icam5*. These findings underscore indications from

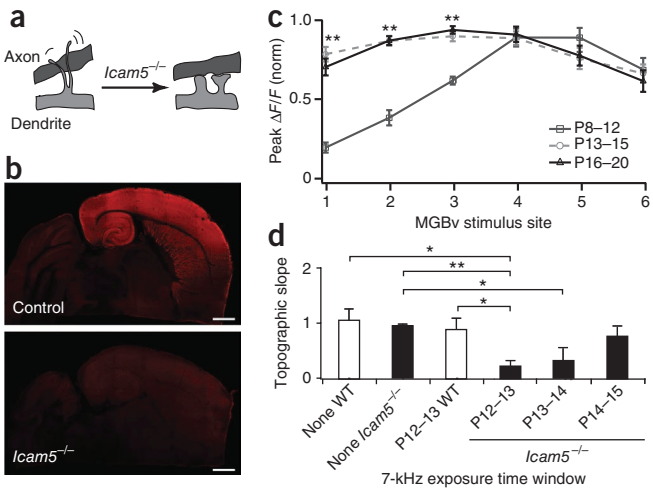

Figure 6 Forebrain-specific gene deletion accelerates thalamocortical plasticity. (**a**) *Icam5* normally slows dendritic spine maturation[21]. (**b**) *Icam5* expression at P13 in the auditory thalamocortical slice. Note the absence of immunostaining in control MGBv and throughout *Icam5*$^{-/-}$ brain. Scale bars represent 1 mm. (**c**) Normalized (norm.) peak $\Delta F/F$ as a function of MGBv stimulus site in *Icam5*$^{-/-}$ mice for three age groups (median ± s.e.m.; P8–12, $n = 8$; P13–15, $n = 10$; P16–20, $n = 9$). $^{**}P < 0.01$ (Mann-Whitney U test) between dark gray and black. (**d**) Topographic slope (median ± s.e.m.) for mice without (none; wild type (WT), $n = 15$; *Icam5*$^{-/-}$, $n = 9$) or after 7-kHz exposure between P12–13 (wild type, $n = 9$; *Icam5*$^{-/-}$, $n = 7$), P13–14 (*Icam5*$^{-/-}$, $n = 9$) or P14–15 (*Icam5*$^{-/-}$, $n = 9$). $^{*}P < 0.05$ (Mann-Whitney U test).

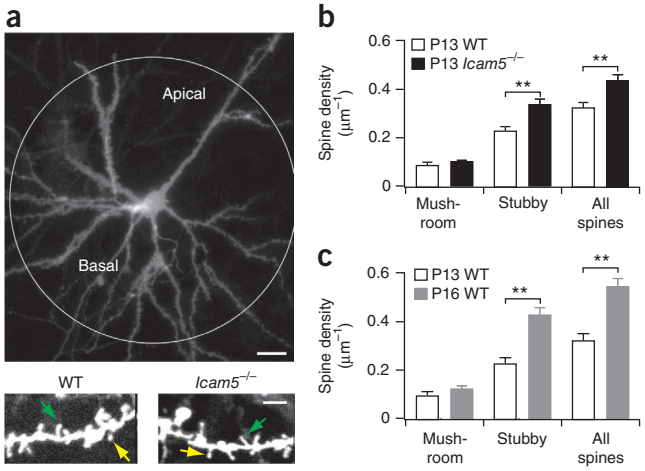

Figure 7 Stubby spine density increases through the critical period. (**a**) Sample DiI-labeled upper L4 pyramidal cell. The white circle denotes a radius of 100 μm around the somata, in which spines were counted. Scale bar represents 20 μm (top). High-power image of dendrites at P13 revealing mushroom (yellow arrows) and stubby spines (green arrows). Scale bar represents 5 μm (bottom). (**b**) Spine density in P13 wild-type ($n = 6$) and *Icam5*$^{-/-}$ mice ($n = 7$ neurons). (**c**) Spine density (median ± s.e.m.) in P13 ($n = 6$) and P16 wild-type mice ($n = 7$ neurons). $^{**}P < 0.01$ (Mann-Whitney *U* test).

wild-type mice that the tonotopic critical period directly reflects a transition in the maturational state of thalamocortical connections[22].

Stubby spine density increases through the critical period

Given that *Icam5* slows filopodia-to-spine transitions[21], we examined whether enhanced spinogenesis might contribute to the accelerated critical period plasticity in *Icam5*$^{-/-}$ mice. Dendritic spines in L4 in a 100-μm radius around cortical pyramidal cell somata have been reported to receive direct thalamocortical input (**Fig. 7a**)[23]. Spines in this region were significantly more dense at P13 in *Icam5*$^{-/-}$ mice than in wild-type mice (spine density: wild type, 0.32 ± 0.02 μm^{-1}, $n = 6$ neurons and 1,777 spines; *Icam5*$^{-/-}$, 0.42 ± 0.02 μm^{-1}, $n = 7$ neurons and 2,567 spines; $P = 0.0012$, Mann-Whitney *U* test; **Fig. 7b**).

Notably, this increase was significant only for stubby spines (wild-type density, 0.24 ± 0.02 μm^{-1}, $n = 1{,}277$ spines; *Icam5*$^{-/-}$ density, 0.33 ± 0.02 μm^{-1}, $n = 1{,}992$ spines; $P = 0.001$, Mann-Whitney *U* test), which are preferentially targeted by MGBv thalamic afferents[23]. Similarly in wild-type mice, a later increase in stubby spine density was eventually observed by P16, marking the end of their typical critical period for tonotopic plasticity (0.44 ± 0.03 μm^{-1}, $n = 7$ neurons and 2,534 spines; **Fig. 7c**). Thus, dendritic spine maturation on thalamo-recipient cortical neurons is a likely locus defining the temporal window for topographic map plasticity in A1.

DISCUSSION

We identified with ever-finer resolution a developmental plasticity occurring at thalamocortical connections related to tonotopy in A1. Accelerated refinement in the absence of the forebrain-specific molecule *Icam5* and the stability of MGBv *in vivo* on tone exposure both support the view that this critical period reflects dendritic spine maturation on L4 neurons in A1.

Previously, tonotopy has primarily been assessed by micro-electrode recording of spiking activity in response to a given tone[5,12]. The resultant best frequency maps exhibited relatively precise point-to-point correlation between tone frequency and its preferred site in the cortical map (**Figs. 1** and **2**). In contrast, VSDI in a slice preparation revealed that stimulation of a point in MGBv recruits peak activity from a broad swath of the A1 map that reflects primarily subthreshold, monosynaptic activation rather than polysynaptic intra-cortical excitation (**Fig. 5b**). The same discrepancy is observed in rodent barrel cortex, where *in vivo* microelectrode recordings have suggested that there is a highly focused mapping between a single whisker and its corresponding barrel[24], whereas *in vivo* VSDI or intrinsic signal imaging have shown that stimulation of a single whisker can evoke substantial activity across a much broader area of the barrel cortex[25–27].

Both somatosensory imaging studies and our own data in A1 (ref. 13) confirm that the spatial peak of the subthreshold activity profile closely corresponds to the map of preferred stimuli obtained with microelectrode mapping. This supports our use of VSDI peak and its topographic slope to track developmental and experiential changes in thalamocortical function and to relate these changes to observations made through conventional mapping of best frequencies (**Figs. 1** and **2**). At the single-cell level, direct whole-cell recordings of synaptic strength across ages further corroborated the use of VSDI peak measurements (**Supplementary Fig. 3**). Our imaging approach therefore provides the appropriate spatial resolution for bridging the gap between *in vivo* network and *in vitro* cellular observations of plasticity mechanism in the developing auditory system.

With its submillisecond time resolution, VSDI further revealed the sequence of activation in a given zone; for example, across the topographic extent of A1 (ref. 13) or along a cortical column. This technique can therefore resolve fast monosynaptic connections from the thalamus and slower, polysynaptic intracortical inputs. During maturation[17,19], deeper regions consisting of the subplate, a transient neocortical structure present in several cortical areas early in development, are largely replaced by the cortical plate, in particular L6. Subplate neurons send strong excitatory projections up to L4, which may regulate activity-dependent processes that catalyze the maturation and plasticity of the developing cortex[19].

At the cellular level, the mechanism of plasticity is related to stubby spine maturation proximal to the soma. These spines have been identified as the direct targets of thalamocortical axons[23] and may underlie the change in thalamocortical connection strength. The critical period profile can be manipulated by acting on this process directly. Our results support the idea that there is accelerated morphological and functional plasticity in the absence of *Icam5*. Our results are consistent with the spine pruning and regrowth that are characteristic of other critical periods, such as in the visual cortex[28]. Conversely, in the latter system, GABA circuits have been implicated in the onset, and various structural brakes, such as peri-neuronal nets or myelin-related signaling, in the closure of plasticity[29]. It will be interesting to determine the extent to which these mechanisms apply in A1.

Consistent with observations made for brainstem tonotopy[30], thalamocortical topography was already organized at hearing onset (**Fig. 3**). Thus, topographic organization is established before sensory experience. By VSDI of subthreshold input, topography *in vitro* is well correlated with tonotopy *in vivo*[13]. As we found, both were modified during a brief critical period from P12–15 in mice exposed to abnormal acoustic environments. In rats, such plasticity is known to impair the perception of the over-represented frequency while improving the discrimination of immediately adjacent frequencies[31].

The critical period for topographic plasticity defined here can be predicted by examining the day-by-day development of connectivity in normally reared animals. During this maturation process, the direct cortical targets of thalamic input shift from deeper regions to L4 (**Fig. 5**), where the number of stubby spines nearest the soma increased significantly ($P = 0.0004$, Mann-Whitney *U* test). The temporal overlap of these changes in L4 may largely contribute to the *in vivo* tonotopic map reorganization

following passive tone exposure (**Fig. 1**), given the lack of tonotopic map changes in the MGBv (**Fig. 2**). However, this does not preclude additional changes at other intracortical sites during the critical period, such as potential refinement of local excitatory-inhibitory balance[32,33]. Detailed analysis of the developing cortical microcircuit, as has already been presented for the mature auditory cortex[34], will be informative.

Isolating a developmental plasticity at the thalamocortical connection does not preclude potential changes in other subcortical regions reflecting auditory experience. Indeed, auditory plasticity has been reported in the midbrain and brainstem circuits, but has typically been associated with sensorineural hearing loss[30,35] or prolonged stimulus manipulations[36–39]. It has yet to be determined whether subcortical reorganization occurs there *de novo* or is brought about by changes first arising in A1 that are then reflected in midbrain or brainstem nuclei via corticofugal inputs[40,41]. The auditory cortex itself is known to exhibit sequential critical periods beyond tonotopy[6,42,43]. For example, following the closure of a critical period for tonotopic map reorganization, we continued to observe rearing-induced changes in tuning bandwidth. Notably, the latter changes were observed not only in A1, but also in the MGBv (**Supplementary Fig. 1**). Thus, it will be important to understand how subsequent stages of plasticity are related to the initial refinement of thalamocortical connections.

METHODS

Methods and any associated references are available in the online version of the paper at http://www.nature.com/natureneuroscience/.

Note: Supplementary information is available on the Nature Neuroscience website.

ACKNOWLEDGMENTS

Icam5$^{-/-}$ mice and antibody were kindly provided by M. Mishina (University of Tokyo) and Y. Yoshihara (RIKEN BSI), respectively. We thank M. Nakamura, A. Takesian, N. Gogolla, E.-J. Yang, K. Quast, M. Marcotrigiano, M. Kelly, R. Pavlyuk, B. Jones O'Brien and V. Khatri for technical assistance and comments. This work was supported by Core Research for Evolutional Science and Technology, Japan Science and Technology Agency (T.K.H.), the Human Frontiers Science Program (T.K.H.), the National Institute on Deafness and Other Communication Disorders (grant 009836, D.B.P.) and the Harvard Society of Fellows (T.R.B.).

AUTHOR CONTRIBUTIONS

T.R.B. performed all of the *in vitro* experiments and analysis. D.B.P. performed or supervised the *in vivo* experiments and analysis. T.R.B., D.B.P. and T.K.H. designed the study and wrote the paper.

COMPETING FINANCIAL INTERESTS

The authors declare no competing financial interests.

Published online at http://www.nature.com/natureneuroscience/.
Reprints and permissions information is available online at http://www.nature.com/reprints/index.html.

1. Hensch, T.K. Critical period regulation. *Annu. Rev. Neurosci.* **27**, 549–579 (2004).
2. Keuroghlian, A.S. & Knudsen, E.I. Adaptive auditory plasticity in developing and adult animals. *Prog. Neurobiol.* **82**, 109–121 (2007).
3. Werker, J.F. & Tees, R.C. Speech perception as a window for understanding plasticity and commitment in language systems of the brain. *Dev. Psychobiol.* **46**, 233–251 (2005).
4. Sanes, D.H. & Bao, S. Tuning up the developing auditory CNS. *Curr. Opin. Neurobiol.* **19**, 188–199 (2009).
5. de Villers-Sidani, E., Chang, E.F., Bao, S. & Merzenich, M.M. Critical period window for spectral tuning defined in the primary auditory cortex (A1) in the rat. *J. Neurosci.* **27**, 180–189 (2007).
6. Insanally, M.N., Kover, H., Kim, H. & Bao, S. Feature-dependent sensitive periods in the development of complex sound representation. *J. Neurosci.* **29**, 5456–5462 (2009).
7. King, A.J. & Nelken, I. Unraveling the principles of auditory cortical processing: can we learn from the visual system? *Nat. Neurosci.* **12**, 698–701 (2009).
8. Wiesel, T.N. & Hubel, D.H. Comparison of the effects of unilateral and bilateral eye closure on cortical unit responses in kittens. *J. Neurophysiol.* **28**, 1029–1040 (1965).
9. Hensch, T.K. Critical period plasticity in local cortical circuits. *Nat. Rev. Neurosci.* **6**, 877–888 (2005).
10. Winer, J.A., Miller, L.M., Lee, C.C. & Schreiner, C.E. Auditory thalamo-cortical transformation: structure and function. *Trends Neurosci.* **28**, 255–263 (2005).
11. Cruikshank, S.J., Rose, H.J. & Metherate, R. Auditory thalamocortical synaptic transmission *in vitro*. *J. Neurophysiol.* **87**, 361–384 (2002).
12. Zhang, L.I., Bao, S. & Merzenich, M.M. Disruption of primary auditory cortex by synchronous auditory inputs during a critical period. *Proc. Natl. Acad. Sci. USA* **99**, 2309–2314 (2002).
13. Hackett, T.A., Rinaldi Barkat, T., O'Brien, B.J., Hensch, T.K. & Polley, D.B. Linking topography to tonotopy in mouse auditory cortex. *J. Neurosci.* **31**, 2983–2995 (2011).
14. Winer, J.A., Sally, S.L., Larue, D.T. & Kelly, J.B. Origins of medial geniculate body projections to physiologically defined zones of rat primary auditory cortex. *Hear. Res.* **130**, 42–61 (1999).
15. Kaur, S., Rose, H.J., Lazar, R., Liang, K. & Metherate, R. Spectral integration in primary auditory cortex: laminar processing of afferent input, *in vivo* and *in vitro*. *Neuroscience* **134**, 1033–1045 (2005).
16. Alford, B.R. & Ruben, R.J. Physiological, behavioral and anatomical correlates of the development of hearing in the mouse. *Ann. Otol. Rhinol. Laryngol.* **72**, 237–247 (1963).
17. Allendoerfer, K.L. & Shatz, C.J. The subplate, a transient neocortical structure: its role in the development of connections between thalamus and cortex. *Annu. Rev. Neurosci.* **17**, 185–218 (1994).
18. Kanold, P.O. & Luhmann, H.J. The subplate and early cortical circuits. *Annu. Rev. Neurosci.* **33**, 23–48 (2010).
19. Zhao, C., Kao, J.P.Y. & Kanold, P.O. Functional excitatory microcircuits in neonatal cortex connect thalamus and layer 4. *J. Neurosci.* **29**, 15479–15488 (2009).
20. Nakamura, K. *et al.* Enhancement of hippocampal LTP, reference memory and sensorimotor gating in mutant mice lacking a telencephalon-specific cell adhesion molecule. *Eur. J. Neurosci.* **13**, 179–189 (2001).
21. Matsuno, H. *et al.* Telencephalin slows spine maturation. *J. Neurosci.* **26**, 1776–1786 (2006).
22. de Villers-Sidani, E. *et al.* Manipulating critical period closure across different sectors of the primary auditory cortex. *Nat. Neurosci.* **11**, 957–965 (2008).
23. Richardson, R.J., Blundon, J.A., Bayazitov, I.T. & Zakharenko, S.S. Connectivity patterns revealed by mapping of active inputs on dendrites of thalamo-recipient neurons in the auditory cortex. *J. Neurosci.* **29**, 6406–6417 (2009).
24. Simons, D.J. Response properties of vibrissa units in rat SI somatosensory neocortex. *J. Neurophysiol.* **41**, 798–820 (1978).
25. Masino, S.A., Kwon, M.C., Dory, Y. & Frostig, R.D. Characterization of functional organization within rat barrel cortex using intrinsic signal optical imaging through a thinned skull. *Proc. Natl. Acad. Sci. USA* **90**, 9998–10002 (1993).
26. Kleinfeld, D. & Delaney, K.R. Distributed representation of vibrissa movement in the upper layers of somatosensory cortex revealed with voltage-sensitive dyes. *J. Comp. Neurol.* **375**, 89–108 (1996).
27. Petersen, C.C., Grinvald, A. & Sakmann, B. Spatiotemporal dynamics of sensory responses in layer 2/3 of rat barrel cortex measured in vivo by voltage-sensitive dye imaging combined with whole-cell voltage recordings and neuron reconstructions. *J. Neurosci.* **23**, 1298–1309 (2003).
28. Mataga, N., Mizuguchi, Y. & Hensch, T.K. Experience-dependent pruning of dendritic spines in visual cortex by tissue plasminogen activator. *Neuron* **44**, 1031–1041 (2004).
29. Morishita, H. & Hensch, T.K. Critical period revisited: impact on vision. *Curr. Opin. Neurobiol.* **18**, 101–107 (2008).
30. Kandler, K., Clause, A. & Noh, J. Tonotopic reorganization of developing auditory brainstem circuits. *Nat. Neurosci.* **12**, 711–717 (2009).
31. Han, Y.K., Köver, H., Insanally, M.N., Semerdjian, J.H. & Bao, S. Early experience impairs perceptual discrimination. *Nat. Neurosci.* **10**, 1191–1197 (2007).
32. Dorrn, A.L., Yavan, K., Barker, A.J., Schreiner, C.E. & Froemke, R.C. Developmental sensory experience balances cortical excitation and inhibition. *Nature* **465**, 932–936 (2010).
33. Sun, Y.J. *et al.* Fine-tuning of pre-balanced excitation and inhibition during auditory cortical development. *Nature* **465**, 927–931 (2010).
34. Oviedo, H.V., Bureau, I., Svoboda, K. & Zador, A.M. The functional asymmetry of auditory cortex is reflected in the organization of local cortical circuits. *Nat. Neurosci.* **13**, 1413–1420 (2010).
35. Harris, J.A. & Rubel, E.W. Afferent regulation of neuron number in the cochlear nucleus: cellular and molecular analyses of a critical period. *Hear. Res.* **216–217**, 127–137 (2006).
36. Smith, Z.D., Gray, L. & Rubel, E.W. Afferent influences on brainstem auditory nuclei of the chicken: n. laminaris dendritic length following monaural conductive hearing loss. *J. Comp. Neurol.* **220**, 199–205 (1983).
37. Seidl, A.H. & Grothe, B. Development of sound localization mechanisms in the mongolian gerbil is shaped by early acoustic experience. *J. Neurophysiol.* **94**, 1028–1036 (2005).
38. Sanes, D.H. & Constantine-Paton, M. Altered activity patterns during development reduce neural tuning. *Science* **221**, 1183–1185 (1983).
39. Mogdans, J. & Knudsen, E.I. Site of auditory plasticity in the brain stem (VLVp) of the owl revealed by early monaural occlusion. *J. Neurophysiol.* **72**, 2875–2891 (1994).
40. Yan, W. & Suga, N. Corticofugal modulation of the midbrain frequency map in the bat auditory system. *Nat. Neurosci.* **1**, 54–58 (1998).
41. Bajo, V.M., Nodal, F.R., Moore, D.R. & King, A.J. The descending corticocollicular pathway mediates learning-induced auditory plasticity. *Nat. Neurosci.* **13**, 253–260 (2010).
42. Popescu, M.V. & Polley, D.B. Monaural deprivation disrupts development of binaural selectivity in auditory midbrain and cortex. *Neuron* **65**, 718–731 (2010).
43. Razak, K.A., Richardson, M.D. & Fuzessery, Z.M. Experience is required for the maintenance and refinement of FM sweep selectivity in the developing auditory cortex. *Proc. Natl. Acad. Sci. USA* **105**, 4465–4470 (2008).

ONLINE METHODS

***In vivo* electrophysiology.** All experimental procedures were carried out according to Harvard and Vanderbilt University animal care and use guidelines. A1 and MGBv recordings were made from the left hemisphere at P28–40. Mice were brought to a surgical plane of anesthesia using a combination of pentobarbital sodium (50 mg per kg of body weight followed by 10–15 mg per kg supplements as needed) and chlorprothixene (0.2 mg). Multi-unit responses were recorded from the middle cortical layers of A1 (420–440 μm from pial surface) with epoxylite-coated tungsten microelectrodes (2.0 MΩ at 1 kHz, FHC) and from MGBv with 16-channel silicon probes (177-μm^2 contact area, 50-μm inter-contact separation, Neuronexus Technologies). Frequency response areas were measured with pseudo-randomly presented tone pips of variable frequency (5.5 to 45.3 kHz in 0.1-octave increments, 20-ms duration, 5 ms raised cosine onset/offset ramps, 0.6-s intertrial interval, one presentation per unique tone/level combination) and level (0–60 dB SPL in 5-dB increments) delivered from a free field electrostatic speaker placed 12 cm from the contralateral ear.

Best frequency was defined for each recording site as the tone frequency that evoked the greatest number of spikes. A1 was readily identified by a clear caudal-to-rostral low-to-high best frequency gradient and was bounded by sharp best frequency reversals or unresponsive sites as described previously[13,44]. A topographic analysis of best frequencies was achieved by dividing the map into equal thirds along the caudal-to-rostral extent and separately analyzing best frequencies in each sector (**Figs. 1f**,**g** and **2f**). No significant differences were found in the spatial sampling density in each sector of the map, justifying comparisons of overall best frequency distributions between groups ($P = 0.56$ for P11–15 versus no exposure and $P = 0.29$ for P16–20 versus no exposure, χ^2 test).

For MGBv, a multi-channel silicon probe was inserted under stereotaxic guidance at the same dorsoventral angle used for the brain slice preparation to effectively isolate it from other thalamic subdivisions. This was confirmed by carefully noting a reversal in the best frequency gradient marking the medial edge of MGBv and by *post mortem* reconstruction of electrode tracks and lesion sites according to previously described methods[13].

Acute auditory thalamocortical slice preparation. C57BL/6J (Jackson Labs) or *Icam5*$^{-/-}$ mice (P8–20, courtesy of M. Mishina, University of Tokyo) were rapidly decapitated without anesthesia and placed in ice-cold ACSF. Slices were sectioned on a vibratome (Microm HM 650V, Thermo Scientific) according to a previously described method[11]. Briefly, 600-μm-thick horizontal slices with the lateral end raised 15°, were cut in ice-cold ACSF and incubated at 35 °C for at least 15 min, before returning to 20–22 °C. One left hemisphere slice was used per animal. The ACSF contained 125 mM NaCl, 25 mM glucose, 25 mM $NaHCO_3$, 2.5 mM KCl, 2 mM $CaCl_2$, 1.25 mM NaH_2PO_4 and 1 mM $MgCl_2$ (315–328 mOsm).

VSDI. The voltage-sensitive dye Di-4-ANEPPS (Invitrogen catalog #D-1199), dissolved at 0.01 mg ml^{-1} in dimethylsulfoxide stock solution, was diluted (0.6 μl ml^{-1}) in ACSF to a final solution of 5 μg l^{-1} Di-4-ANEPPS. Slices were incubated for at least 90 min before transfer to an ACSF (20–22 °C) recording chamber. Slices were imaged using an Olympus MVX10 microscope with 1× 0.25 numerical aperture objective. Excitation light from a shuttered 150-W halogen lamp (MHF-G150LR, Moritex) was band-pass filtered (515 and 535 nm) and reflected toward the sample by a 570-nm dichroic mirror. Emitted fluorescence, reflecting a change in potential across neuronal membranes[45,46] (**Supplementary Fig. 3**), was long-pass filtered (590 nm) and imaged using a MiCam Ultima CMOS-based camera (SciMedia). Fluorescent changes (1-ms frame rate for 512-ms periods) were averaged across ten trials and integrated across different regions of interest containing 5 × 5 pixels covering 125 × 125 μm by spatial averaging and across different trials using MiCam Ultima analysis software.

Individual time course traces were subsequently exported to Igor Pro (WaveMetrics) to combine data for a number of slices. Fluorescence change was normalized to resting fluorescence ($\Delta F/F_0$). Stimulation was controlled by a programmable pulse generator (MiCam Ultima software, SciMedia) linked to a constant current stimulus isolation unit (Iso-Flex, A.M.P.I.). Discrete sites in the MGBv were activated with an ACSF-filled patch pipette (0.5 mA, 1-ms pulse) at 100 ms after recording onset.

Response amplitude was defined as maximum fluorescence change ($\Delta F/F$) per trial at a given region of interest. Peak amplitude was defined as maximum response amplitude across all L4 locations. Variations in daily preparation were normalized by slice; all signals were divided by the maximum change in fluorescence measured in a set of experiments:

$$\text{Normalized } \Delta F/F = \frac{\Delta F/F}{\max(\Delta F/F)}$$

Response latency was defined as the time elapsed from stimulus pulse to half-maximal signal amplitude. As VSDI reports relative changes in fluorescence as a function of membrane potential fluctuation[45], the absolute changes in fluorescence might reflect a number of technical, as well as biological, considerations (such as differential staining and transparency). Thus, our VSDI results are presented as normalized signals for comparison across ages and conditions.

The strongest signals as a function of MGBv stimulus site were taken from regions of interest along the rostro-caudal axis of A1 at a constant distance from an anatomical landmark chosen as reference (most rostral point X of hippocampus in **Supplementary Fig. 5**) and at constant depth from the pia, corresponding to upper L4 on the basis of Nissl stains (**Fig. 5a**), covering a total distance of 2,250 μm. The stimulating electrode was positioned on the rostral MGBv at six discrete positions spaced at 100-μm intervals along the medio-lateral axis (landmark 4 for stimulus site 1; **Supplementary Fig. 5**)[13].

For columnar analysis, regions of interest in which the signal in upper L4 was strongest were chosen along the medio-lateral A1 axis orthogonal to the pia, for a total distance of 1,000 μm. The stimulating electrode was placed in the most rostral part of the MGBv in which the stimulus could evoke the strongest response in A1 (landmark 5; **Supplementary Fig. 5**). To assess any polysynaptic contribution, we used a modified ACSF with high divalent cation (X^{2+}) content[11]: 115 mM NaCl, 25 mM glucose, 25 mM $NaHCO_3$, 2.5 mM KCl, 7.2 mM $CaCl_2$ and 4.2 mM $MgCl_2$ (315–325 mOsm). To confirm the synaptic nature of the response, we added 40 μM D(−)-2-amino-5-phosphonovaleric acid and 10 μM 6-cyano-7-nitroquinoxaline-2,3-dione to the ACSF at the end of most experiments (**Supplementary Fig. 2b**).

Sound exposure. Subsets of mouse pups and mothers were placed in a sound-attenuating chamber (IAC) and exposed to 7- or 20-kHz tones (100-ms pulses at 5 Hz[47,48] for 1 s, followed by 2 s of silence, 78 or 73 dB SPL, respectively). A 7-kHz frequency was chosen as the middle of the sound spectrogram for mouse pup wriggling calls[49], and therefore ethological for mice of this age. Mice were otherwise reared under standard conditions (12:12 h light:dark cycle, access to water and food *ab libitum*) and moved about freely in their cage. Audible (7 kHz) tones were generated by Audacity software (http://audacity.sourceforge.net/) and amplified by speakers placed in two corners of the chamber. High-frequency (20 kHz) tones were generated by Adobe Audition software and amplified by an electrostatic speaker driver (ED1) and electrostatic speaker (ES1, Tucker Davis Technologies) placed on top of the mouse cage.

Subsets of mice were exposed to 7-kHz tones from P8 until recording (removed less than 30 min before decapitation) around P20 (P19–21). Other subsets were exposed for shorter time windows, P8 to P11, P12 to P15, P16 to P19, P12 to P13, P13 to P14, P14 to P15, P12 to P14 or P13 to P15, and were then returned to standard housing conditions until decapitation around P20 for VSDI.

DiI labeling. C57BL/6J mice at P13 or P16 (Jackson Lab) or *Icam5*$^{-/-}$ mice at P13 were anesthetized with nembutal (50 mg per kg) and killed by transcardial perfusion with 0.9% saline (wt/vol) and 4% paraformaldehyde (wt/vol) in phosphate-buffered saline (PBS). Brains were trimmed and thalamocortical slices were cut (200 μm thick) for 'DiOlistics' labeling with lipophilic dye (DiI, Molecular Probes) coated on tungsten particles (0.7-μm diameter, Bio-Rad)[50]. Density of labeling was controlled by gas pressure (200-psi helium) and no other filters. Randomly labeled pyramidal neurons situated in upper L4 of A1 were selected by confocal microscopy (40× air objective, 3× zoom; FluoView1000, Olympus). Images at 0.25-μm steps were acquired and stacked for three-dimensional reconstruction using FluoView software. Neurites were reconstructed in a radius of 100 μm from the soma using Neurolucida (MicroBrightField). All protrusions along apical and basal dendrites were counted. Those with distinct heads and head diameter larger than neck diameter were classified as mushroom spines, whereas dendritic protrusions without distinct heads were classified as stubby spines[23]. Spines that were thinner than 0.3 μm and longer than 2 μm, defined as filopodia or thin spines, were not counted.

Immunohistochemistry. Standard protocols were used to label thalamocortical slices. Briefly, slices (600 and 100 µm thick for Nissl and Icam5 staining, respectively) were kept in 4% paraformaldehyde overnight at 20–22 °C, washed in PBS, solubilized, blocked in 0.8% Triton X-100 (wt/vol) and 20% bovine serum albumin (BSA, wt/vol) in PBS (4 °C overnight), and incubated for Nissl stain with NeuroTrace 435/455 (Molecular Probes) or rabbit polyclonal antibody to *Icam5* (courtesy of Y. Yoshihara, RIKEN BSI)[21] in 5% BSA in PBS (4 °C overnight), followed by a fluorescent secondary antibody.

***In vitro* patch-clamp recording.** Slice preparation and stimulation protocols were as described for the VSDI experiments. Whole-cell recordings of upper L4 pyramidal neurons were amplified using Axopatch 200B amplifiers (Axon Instruments, Molecular Devices). Voltages (in current-clamp mode) were recorded with pipettes containing 120 mM potassium gluconate, 10 mM KCl, 4 mM ATP-MG, 10 mM phosphocreatine, 0.3 mM GTP, 10 mM HEPES and 0.2% biocytin (wt/vol, pH 7.3, 290 mOsm). For each slice, up to three cells per stimulus site (1, 3 and 5) and L4 location (8, 10 and 13, respectively) were patched, and the cell with the strongest response (average of 30 traces, clamped at −70 mV) was used for the analysis.

Statistical analyses. Results are reported as mean ± s.e.m. and compared across groups using a two-tailed, unpaired Student's *t* test with statistical significance at $P < 0.05$ if n was bigger than 10, where n represents the number of animals or neurons for **Figures 1**, **2** and **7**, per experiment. For small data samples ($n < 10$), or where the assumption of a Gaussian distribution could not be verified, results were reported as median ± s.e.m., and the nonparametric two-tailed Mann-Whitney *U* or Wilcoxon rank sum test was used (**Figs. 4e**, **5b**, **6** and **7** and **Supplementary Fig. 3b**) with statistical significance at $P < 0.05$. Input strength distributions (**Fig. 4a**) and gradient of peak locations (**Fig. 4c**) were compared with two-way ANOVA tests. Best frequency distributions (**Figs. 1e** and **2e**) were compared with two-sample Kolmogorov-Smirnov tests.

44. Stiebler, I., Neulist, R., Fichtel, I. & Ehret, G. The auditory cortex of the house mouse: left-right differences, tonotopic organization and quantitative analysis of frequency representation. *J. Comp. Physiol. [A]* **181**, 559–571 (1997).
45. Grinvald, A. & Hildesheim, R. VSDI: a new era in functional imaging of cortical dynamics. *Nat. Rev. Neurosci.* **5**, 874–885 (2004).
46. Ferezou, I., Bolea, S. & Petersen, C.C.H. Visualizing the cortical representation of whisker touch: voltage-sensitive dye imaging in freely moving mice. *Neuron* **50**, 617–629 (2006).
47. Zhou, X., Nagarajan, N., Mossop, B.J. & Merzenich, M.M. Influences of un-modulated acoustic inputs on functional maturation and critical-period plasticity of the primary auditory cortex. *Neuroscience* **154**, 390–396 (2008).
48. Kim, H. & Bao, S. Selective increase in representations of sounds repeated at an ethological rate. *J. Neurosci.* **29**, 5163–5169 (2009).
49. Geissler, D.B. & Ehret, G. Auditory perception vs. recognition: representation of complex communication sounds in the mouse auditory cortical fields. *Eur. J. Neurosci.* **19**, 1027–1040 (2004).
50. Gan, W.B., Grutzendler, J., Wong, W.T., Wong, R.O. & Lichtman, J.W. Multicolor 'DiOlistic' labeling of the nervous system using lipophilic dye combinations. *Neuron* **27**, 219–225 (2000).

doi:10.1038/nn.2882